https://doi.org/10.5194/egusphere-2022-1209
Preprint. Discussion started: 12 January 2023

Evidence of Nitrogen Loss through Anaerobic Ammonium Oxidation Coupled with Ferric Iron Reduction in the Yellow River Wetland

Qingsong Guan* [a,b,c], Tao Li [b,c], Yiqiao Zhou [b,c], Fan Yang [b,c], Qingbin Li[a]

[a] *State key Laboratory of Hydroscience and Engineering, Beijing 100084, China.*

[b] *College of Application of Engineering, Henan University of Science and Technology, Sanmenxia 472000, China.*

[c] *Engineering Technology Research Center of Sanmenxia Yellow River Wetland Environmental Process and Ecological Restoration, Sanmenxia 472000, China.*

*Email:guanqingsong163@163.com

Abstract: Anaerobic ammonium oxidation coupled with iron(III) reduction (Feammox) is a recently discovered pathway of nitrogen removal. However, little is known about the pathways of N transformation via Feammox in the Yellow River wetland. In this study, the difference between Feammox in a natural wetland (site YJW) and a crop rotation wetland (site TEH) was researched using isotope tracing and metagenome techniques. The results revealed that Feammox occurred in TEH but not in YJW. The Feammox rates in the TEH samples were 0.02–0.13 mg N kg^{-1} d^{-1} in different depth intervals (0–5 cm, 5–10 cm, 10–20 cm, and 20–30 cm), and the maximum value for TEH occurred in the 5–10 cm depth interval. Iron reducing bacteria play an essential role in Feammox. Rotational tillage reduced the microbial diversity of the iron-reducing bacteria, but it increased the abundance of iron-reducing bacteria at the genus level, and the dominate iron-reducing bacteria responsible for the Feammox process were *Anaeromyxobacter* and *Geobacter*. The Feammox rate was less than the denitrification rate (0.55–1.09 mg N kg^{-1} d^{-1}), an estimated nitrogen loss of 1.1–7.1 t N km^{-2} a^{-1} was associated with the Feammox in the wetland. However, the correlation between the functional genes of the iron-reducing bacteria and the rate remains unclear. Overall, the co-occurrence of ammonium oxidation and iron reduction

https://doi.org/10.5194/egusphere-2022-1209
Preprint. Discussion started: 12 January 2023

suggest that Feammox can play an essential role in the pathway of nitrogen removal in the Yellow River wetland.

Keywords: Yellow River wetland; Nitrogen removal; Iron-reducing bacteria;

https://doi.org/10.5194/egusphere-2022-1209
Preprint. Discussion started: 12 January 2023

1. Introduction

It is generally believed that denitrification ($NO_3^- \rightarrow NO_2^- \rightarrow NO \rightarrow N_2O \rightarrow N_2$) and anaerobic ammonium oxidation (anammox) ($NH_4^+ + NO_3^- \rightarrow N_2$) reactions are the major pathways of nitrogen removal in ecosystems (Canfield et al., 2010; Dalsgaard et al., 2003; Jensen et al., 2008). Recent studies have identified another significant nitrogen removal pathway, i.e., anaerobic ammonium oxidation coupled with iron (III) reduction (Feammox). Feammox refers to an autotrophic process in which microorganisms are oxidized under anaerobic conditions, with NH_4^+ serving as the electron donor. In addition, the electron acceptor, i.e., Fe(III), is reduced to Fe(II) and energy is obtained. The chemical equations for this process are Eqs. (1)–(3), and Eq. (1) is the major reaction.

$$3Fe(OH)_3 + 5H^+ + NH_4^+ \rightarrow 3Fe_2^+ + 9H_2O + 0.5N_2 , \quad (1)$$

$\Delta_r G_m = -245$ kJ mol^{-1}.

$$6Fe(OH)_3 + 10H^+ + NH_4^+ \rightarrow 6Fe_2^+ + 16H_2O + NO_2^-, \quad (2)$$

$\Delta_r G_m = -164$ kJ mol^{-1}.

$$8Fe(OH)_3 + 14H^+ + NH_4^+ \rightarrow 8Fe_2^+ + 21H_2O + NO_3^-, \quad (3)$$

$\Delta_r G_m = -207$ kJ mol^{-1}.

Such a process was first discovered in the laboratory in 2005, but the Fe(III)–NH_4^+ coupling relationship was not fully illustrated (Clement et al., 2005). Later, scholars conducted culturing experiments using an inorganic carbon source, NH_4^+ as electron donor, and Fe(III) as the electron acceptor and discovered the strong positive correlation between Fe(III) and NH_4^+. This was when the Feammox concept was first proposed (Sawayama, 2006). Through further research, the effect of Feammox on natural ecosystems gradually gained more attention. The characteristics of Feammox in natural ecosystems, including tropical rain forest soil (Yang et al., 2012), paddy

https://doi.org/10.5194/egusphere-2022-1209
Preprint. Discussion started: 12 January 2023

field soil (Ding et al., 2014), the tidal flat wetland in the estuary of the Yangtze River (Li et al., 2015), and riparian soil (Ding et al., 2017), were successively reported. It is gradually becoming recognized that Feammox is a non-negligible process in nitrogen removal in natural ecosystems.

Feammox is driven by iron-reducing bacteria (FeRB). The coupling relationship between FeRB and Feammox has been discovered in natural ecosystems, including paddy soil (Zhou et al., 2016), intertidal wetlands (Li et al., 2015), paddy soil (Ding et al., 2014), deep lake sediments (Melton et al., 2014), arsenic contaminated soil (Somenahally et al., 2011), and a non-sulfide depositional environment (Weber et al., 2006). Characterizing FeRB facilitates our understanding of the Feammox process. Shu et al. (Shu et al., 2016) studied the coexistence mode of nitrogen-iron related bacteria in a waste water processing system.

However, few studies have explored the diversity of the FeRB community in the Yellow River wetland and the interactions between the FeRB community and the Feammox process. The Yellow River is a typical low organic carbon ecosystem (Guan, 2022). The characteristics of the Feammox process in the Yellow River and its contribution to the Yellow River's nitrogen loss remain unknown. In this study, the Yellow River wetland in San Men Xia was studied. The nitrogen isotope tracing and metagenomic techniques were used to investigate the characteristics of the Feammox process in the sediments.

2. Materials and methods

2.1. Site description and sediment sampling

The Sanmenxia Dam was built in 1960. The reservoir adopts the operation mode of storing clear water in winter and spring and discharging the muddy soil and water in summer and autumn, and the wetland changes accordingly. The wetland of the Sanmenxia reservoir is a

https://doi.org/10.5194/egusphere-2022-1209
Preprint. Discussion started: 12 January 2023

representative river-type wetland in northern China (Fig. 1). The wetland is 205 km long and 3 km wide, with a total area of 28,500 hm^2, of which the core area accounts for 14,400 hm^2. The study area contains mountains, valleys, and steep ravines. It has a semi-arid continental monsoon climate. The annual average temperature is 12.8–13.9°C, and the rainfall is concentrated from July to September, with an average annual precipitation of 513–638 mm. The national nature reserve of the Sanmenxia Yellow River wetland is the habitat of the White Swan and is an important water conservation area. Sampling was conducted in August 2021, when the wetland was not flooded. There were two sampling sites. The site was covered with *P. australis* and *T. orientalis* (designated YJW; 110°43′E, 34°37′N), which was a natural biological environment. In the second site (designated THE; 111°8′E, 34°47′N), where periodic planting and harvesting was conducted. The major crops were sunflowers and beans. During the sampling period, the crops had already been harvested. The soil was dry and had a low moist content. The YJW sampling depth intervals were 0–5 cm, 5–10 cm, 10–13 cm, and 13–18 cm. The sediment below 13 cm was sand. The TEH sampling depth intervals were 0–5 cm, 5–10 cm, 10–20 cm, and 20–30 cm, and there was no obvious layering. The sampling scheme was random, and each sample was a mixture of the same layer taken from each site in the scheme. Water samples were collected at the same time as the sediment samples. The sediment samples were placed in sterilized centrifuge tubes and stored on dry ice in preparation for immediate meta genomic analysis. Other sediment samples were immediately placed in zip-lock bags and stored in a portable refrigerator in preparation for indoor analysis. The samples were divided into two parts. One part was used for the immediate isotope culturing experiments. The other part was analyzed to determine the sediment's physiochemical properties. The water samples were immediately pretreated and tested for Fe(III).

https://doi.org/10.5194/egusphere-2022-1209
Preprint. Discussion started: 12 January 2023

2.2. Isotopic tracer incubations

The isotope experiments were conducted in an anaerobic glove box filled with helium. First, ultrapure water was boiled and purged with helium for 10 minutes. Then, the sediments were mixed with ultrapure water at a 1:1 mass ratio according to the wet weight of the sediment. The mixture was stirred while being purged with helium for 10 minutes to produce anaerobic mud. The mud was pre-incubated in an anaerobic glove box for 2 days to remove any residual oxygen, nitrate, and nitrite. After the pre-culture step, 60 mL of mud were transferred into a 100 mL vial. The vial was then sealed with a rubber stopper and an aluminum cap. Three sets of conditions were prepared for the experiments: (1) a control group (sterile water was used in place of $^{15}NH_4Cl$); (2) $^{15}NH_4Cl$ (98% ^{15}N, Sigma–Aldrich, St. Louis, MO, USA); and (3) $^{15}NH_4$ + Fe(III). Subsequently, 100 μL of $^{15}NH_4Cl$ were added using a micro-injector, and the final $^{15}NH_4Cl$ concentration was 100 μmol L^{-1}. To avoid limiting the reactions in (2) and (3), Fe(III) ($FeCl_3$ solution) was added at a 6:1 ratio (Fe(III):$^{15}NH_4^+$). The incubation time was set to 0, 1, 3, 5, 8, and 12 days. At each time point, 200 μL of saturated HgCl solution were injected into the vial to terminate the reactions. $^{29}N_2$ and $^{30}N_2$ were analyzed using an isotope ratio mass spectrometry (IRMS, GasBench II−Delta V Advantage, Thermo Fisher, Bremen, Germany). After the gas samples were collected, the mud samples were analyzed to determine the Fe(II) and dissolved inorganic nitrogen (DIN) contents.

2.3. Metagenomic sequencing

The metagenome sequencing analysis was conducted by Shanghai Mei Ji Biomedical Technology Co., Ltd. The deoxyribonucleic acid (DNA) was extracted from the samples from

https://doi.org/10.5194/egusphere-2022-1209
Preprint. Discussion started: 12 January 2023

each sampled layer. Its purity and concentration were analyzed to understand the sample's integrity. Qualified samples were fragmented to about 400 bp using a Covaris M220 instrument. The final library was obtained after further addition, purification, and polymerase chain reaction (PCR) amplification. Metagenomic sequencing was performed on the final qualified library using the llumina NovaSeq/Hiseq Xten platform.

The raw sequences in the metagenomic dataset were further optimized through splitting, quality shearing, and decontamination. The optimized sequences were then used for the splicing assembly and gene prediction. The resulting genes were then used for the functional annotation and classification using the nonredundant protein (NR), evolutionary genealogy of genes non-supervised orthologous groups (EggNOG), and Kyoto Encyclopedia of Genes and Genomes (KEGG) databases. Multi-directional statistical analysis and data exploration, such as similarity clustering, grouping and ranking, and difference comparison, were conducted on the results of the above analyses.

2.4. Sample analysis

The pH, temperature, and other water parameters were measured using a portable water quality parameter analyzer (DZB-712F). The total nitrogen (TN) content of the water was determined using alkaline potassium persulfate digestion and UV spectrophotometry. The total phosphorus (TP) content was determined through digestion using potassium persulfate and ammonium molybdate spectrophotometry. The NH_4^+, NO_3^-, and NO_2^- contents were determined using a continuous-flow nutrient autoanalyzer (AA3 AutoAnalyzer, Bran+Luebbe GmbH, Norderstedt, Germany). The hydrochloric acid-extractable total iron and hydrochloric acid-

https://doi.org/10.5194/egusphere-2022-1209
Preprint. Discussion started: 12 January 2023

extractable Fe(II) were measured using the ferrozine-staining and UV spectrophotometry (Lovley and Phillips, 1987) methods.

2.5. Statistical analysis

One-way analysis of variance (ANOVA) was conducted to analyze the different physical-chemical properties, the reduction rate of Fe(III), and the difference in the $^{30}N_2$ and $^{29}N_2$ production rates. The significance was α=0.05. All of the data passed the Shapiro-Wilk normality test and the Levene's homogeneity and variance test. No variables needed to be transformed. The Pearson correlation coefficient was used to reveal the relationship between the Fe(III) and $^{29}N_2$ reduction rates. The statistical analysis was conducted using the SPSS 25.0 software (SPSS Inc., Chicago, IL, USA), and the figures were plotted using Origin Pro 8.

3. Results

3.1. Chemical characteristics of the sediments

The water had an alkaline pH level. The conductivity difference was small. The Eh was less than 300 mV, and the water was a moderate reducing environment. The total iron content of the YJW sample was significantly higher than that of the TEH sample. There was no significant difference in the Fe(II) and Fe(III) contents of the YJW sample. The Fe(II) content of the TEH sample was 73%. Nitrate accounted for 90% and 97% of the inorganic nitrogen in the YJW and TEH samples, respectively (Table 1).

The total organic carbon (TOC) contents of the YJW samples were 0.22% to 0.28%. The sample at 13–18 cm was sand, and the TOC content was 0.03%. The inorganic nitrogen was mainly ammonia. The ammonia contents of the YJW and TEH samples were 79% to 94% and 44%

https://doi.org/10.5194/egusphere-2022-1209
Preprint. Discussion started: 12 January 2023

to 90%, respectively. The difference in their iron contents was significant. The iron contents of the YJW samples were dramatically higher than those of the TEH samples. The YJW sample collected at 13–18 cm had a significantly lower iron content than the soil layer. The Fe(II) content of the YJW samples were 6.5% to 60%, whereas the Fe(II) contents of the TEH samples were greater than 60% (Table 2).

3.2. Rates of Feammox

Fig. 2 and 3 show the changes in the $^{29}N_2$ and $^{30}N_2$ concentrations with incubation time for the YJW and the samples, respectively. No isotope gas accumulated in the blank group. The $^{29}N_2$ of the $^{15}NH_4^+$ and $^{15}NH_4^+$ + Fe(III) treatments of the YJW samples accumulated linearly with a low accumulated concentration. No $^{30}N_2$ accumulation was observed. The samples collected at different depths accumulated similar amounts of $^{29}N_2$. The $^{15}NH_4^+$ and $^{15}NH_4^+$ + Fe(III) treatments of the samples accumulated $^{29}N_2$ at a faster rate than those of the corresponding YJW samples. No $^{30}N_2$ accumulation was detected. The existence of Fe(III) increased the isotope accumulation concentration for all of the samples, except the YJW sand sample collected at 13–18 cm. The TEH sample ollected at 5–10 cm had the largest accumulation rate.

$^{29}N_2$ and $^{30}N_2$ were produced through three pathways, i.e., Feammox, anammox, and denitrification (Table 3). The potential Feammox rate was calculated from the data for the $^{15}NH_4^+$ treatment group and the blank group. The Feammox rate was defined as the $^{29}N_2$ and $^{30}N_2$ production rate. The Feammox rate results are presented in Fig. 4. The Feammox rate of the YJW group could only be calculated for the 0–5 cm sample. The Feammox rates of the TEH samples were 0.02–0.13 mg N kg^{-1} d^{-1}, with an average of 0.06 mg N kg^{-1} d^{-1}. The Feammox rate was larger for the surface sediments than for the deeper layer, and the maximum value was detected

https://doi.org/10.5194/egusphere-2022-1209
Preprint. Discussion started: 12 January 2023

for the 5–10 cm sample. The Feammox rates of the Fe(III) treatment were 0.06–0.21 mg N kg^{-1} d^{-1}, with an average of 0.11 mg N kg^{-1} d^{-1} (8.3%).

3.3. Fe(III) reduction rates

The Fe(III) contents of the YJW samples were higher than those of the TEH samples, and Fe(III) content was positively correlated with the iron reduction rate. The reduction rates of the YJW and the control groups were 0–66 mg Fe kg^{-1} d^{-1} and 2–5 mg Fe kg^{-1} d^{-1}, respectively(Fig. 5). The $^{15}NH_4^+$ and Fe(III) promoted iron reduction. There was a large difference between the Fe(III) reduction rates of the samples from the two sites. In general, the Fe(III) reduction rates of the YJW samples were higher than those of the TEH samples. The largest iron reduction rate occurred in the 5–10 cm YJW sample. The reduction rate of the YJW surface sediment was larger than that of the sample from the bottom layer. The Fe(III) reduction rate could not be calculated for the 10–13 cm, 13–18 cm, and iron-free YJW samples. The opposite trend was observed for the TEH samples. The reduction rate of the TEH surface sediment was lower than that of the bottom layer(Fig. 5).

3.4. Feammox Functional Microorganism Abundance Comparison

No microorganisms were detected in the 13–18 cm YJW sample. At the phylum level, *Proteobacteria*, *Acidobacteria*, *Bacteroidetes*, *Actinobacteria*, *Nitrospirae*, *Firmicutes*, and *Cyanobacteria* have been classified as FeRB (Peng et al., 2016) and the distribution of these seven FeRB in the samples were 85.18%, 86.9%, 91.3%, 74.1%, 70.57%, 70.51%, and 66.64%, respectively (Fig. 6). The major phylum of the FeRB communities in the YJW samples was

https://doi.org/10.5194/egusphere-2022-1209
Preprint. Discussion started: 12 January 2023

Proteobacteria, while the major phyla in the TEH samples were *Proteobacteria*, *Acidobacteria*, and *Bacteroid*etes.

The relative abundances of the microbial diversities are shown in Fig. 7. At the genera level, the FeRB detected in this study were *Acidiferrimicrobium*, *Shewanella*, *Anaeromyxobacter*, and *Geobacter*. The dominant genus in the YJW samples was Geobacter, and the dominant genus in the TEH samples was Anaeromyxobacter (Fig. 7). The overall genus abundance of the TEH samples was higher than that of the YJW samples.

4. Discussion

4.1. Occurrence of Feammox

The accumulation of isotope gases indicates the occurrence of the Feammox process in the Yellow River wetland, but the rates at the different sampling sites were dramatically different. The Feammox rate of the YJW site was lower than that of the site. Table 4 shows that the Feammox rate of the Yellow River wetland was lower than that of the other ecosystem. Many factors can affect the Feammox process and rate. The iron and ammonia contents are low in the Yellow River wetland; for example, the Fe(III) and NH_4^+ contents of the Qin Shui shore area were 0.94–1.53 g kg^{-1} and 1.35–2.95 mg kg^{-1}, respectively (Ding et al., 2017). Organic matter can act as an electron shuttle and is beneficial to the Feammox reaction. The organic content of the Yellow River wetland was lower than that of other wetlands (Guan, 2022). Additionally, large gaps exist in the Yellow River wetland, and the redox potential measured in situ is in the range of 446–526 mV, which is not befeficial to Fe(III) reduction. The types and abundance of iron-reducing bacteria are also important limiting factors. The TEH site had a larger genus abundance than the YJW site. *Anaeromyxobacter* and *Geobacter* are two major bacteria that drive Feammox.

https://doi.org/10.5194/egusphere-2022-1209
Preprint. Discussion started: 12 January 2023

Moreover, (Bakermans and Madsen, 2002) have demonstrated that FeRB are considered to be bioremedial agents dueowing to their diverse capabilities in some anoxic environments.

The average Fe(III) content of the YJW samples was 13 times that of the TEH samples, indicating a high Fe(III) reduction rate. However, the Feammox rate was still low. The key reason for this phenomenon is that only a small proportion of the Fe(III) reduction was coupled with Feammox (Fig. 8). Much of the Fe(III) reduction was coupled with the oxidation of the organic matter. In addition, the abundances of the related Feammox bacteria were quantified to reveal the potential mechanisms of the FeRB in order to understand the positive relationship between Fe(III) reduction and Feammox in intertidal wetlands (Li et al., 2015).

4.2. Contribution of Feammox to nitrogen loss

To calculate the nitrogen loss resulting from Feammox, the nitrogen isotope tracing technique was used to analyze the denitrification and anammox rate (see Appendix I). The dominant pathway of nitrogen loss in the Yellow River wetland was denitrification, and its rate was higher than those of Feammox and anammox (Figs. A1, A2, and A3). Rotational planting and harvesting changed the original physical-chemical properties and the microbial community of the wetland. The denitrification rate of the YJW site was higher than that of the TEH site. The metagenomic results revealed that the abundances of denitrification genes, i.e., *nir*S, *nor*B, and *nos*Z, was higher in the YJW site than in the TEH site (Fig. A4). The denitrification process consumed the majority of the NO_3^- and NO_2^-, which made NH_4^+ the most concentrated inorganic nitrogen in the sediment. The denitrification in the TEH sitewas relatively weak, and thus, the nitrate content was similar to the ammonia nitrogen content.

The nitrogen loss resulting from Feammox was small (Fig. 9). The percentage of nitrogen loss resulting from Feammox in the YJW site was less than 3% (T=total nitrogen loss =

https://doi.org/10.5194/egusphere-2022-1209
Preprint. Discussion started: 12 January 2023

denitrification + anammox + Feammox). The nitrogen loss resulting from Feammox in the TEH site was 21–72%, with an average of 42%. The nitrogen losses resulting from Feammox in the mangrove wetland (Guan et al., 2018), paddy field soil (Ding et al., 2014), Yangtze River estuary wetland (Li et al., 2015), and Taihu riparian zone (Ding et al., 2017) were 6.4%, 3.9–31%, 3.1–4.9%, and 4–7.3%, respectively. The density of the Yellow River wetland was 1.5 g/cm^3. Conservatively speaking, the nitrogen loss resulting from Feammox in the 0–10 cm sediment was 1.1–7.1 t N km^{-2} a^{-1}, which is lower than the nitrogen loss in the Yangtze River. The total area of the Yellow River wetland in Sanmenxia was 28,500 hectares, and the total nitrogen loss resulting from Feammox in the wetland was 313.5–2023.5 t N a^{-1}.

4.3. Diversity of iron-reducing bacteria communities

Iron-reducing bacteria are considered to be key microorganisms and can influence the nitrogen distribution and conversation in soil (Bongoua-Devisme et al., 2013). Researchers have found that iron-reducing bacteria are closely related to Feammox using molecular biology techniques. Microorganisms such as Geobacter and Anaeromyxobacter are the major bacteria that drive the Feammox process (Zhou et al., 2016). Li et al. (Li et al., 2015) suggested that *Geobacter* and *Shewanella* may drive the Feammox process. Other studies have speculated that *Acidimicrobiaceae* (Huang and Jaffé, 2015) may play an important role in driving the Feammox process in forested riparian wetlands, but so far only one isolate, namely, *Acidimicrobiaceae sp. A6*, has been identified as performing the Feammox process (Huang et al., 2018).

Different plant coverage leads to different bacterial communities (Wang and Li, 2011). The major plants in the YJW site were reeds and cattails. The crops grown in the TEH site reduced the abundances of iron-reducing bacteria. However, the genus abundance in the TEH site was

https://doi.org/10.5194/egusphere-2022-1209
Preprint. Discussion started: 12 January 2023

higher than that in the YJW site, which was the key reason for the higher Feammox rate in the TEH site. *Anaeromyxobacter* and *Geobacter* were the major Feammox-driving bacteria. However, many facts are still unclear regarding the functional genes of the iron-reducing bacteria. The genes related to Fe(III) metabolism were analyzed (Fig. 10). The functional genes were more abundant in the YJW site, leading to a higher iron reduction rate.

5. Conclusions

In conclusion, the occurrence of Feammox in the Yellow River wetland, Sanmenxia, was proven using isotope tracing and metagenomic techniques, but large differences in the process existed in the different areas of the wetlands. Rotational planting and harvesting increased the abundances of the iron-reducing bacteria, which led to a higher Feammox rate and a nitrogen loss of 21–27%. Denitrification was the dominant pathway of nitrogen loss, and it was associated with higher functional gene abundances. Our results demonstrate that FeRB play a vital role in the Feammox process, which can be influenced by the type of wetland. *Anaeromyxobacter* and Geobacter may be the major genus driving Feammox, but the functional genes leading to Feammox remain unclear. In addition, the total nitrogen loss rate as a result of Feammox was estimated to be 1.1–7.1 t N km^{-2} a^{-1}. The total nitrogen loss in the basin was about 313.5–2023.5 t N a^{-1}. The results of this study provide new insights into the transformation and cycling of N in the Yellow River wetland.

Declaration of Competing Interest

The authors declare that they have no known competing financial interests or personal relationships that could have appeared to influence the work reported in this paper.

Acknowledgements

https://doi.org/10.5194/egusphere-2022-1209
Preprint. Discussion started: 12 January 2023

This research was supported by the Open Research Fund Program of the State Key Laboratory of Hydroscience and Engineering (sklhse-2021-C-05). We also thank the reviewers for their constructive suggestions.

References

Bakermans, C., Madsen, E.L., 2002. Diversity of 16S rDNA and naphthalene dioxygenase genes from coal-tar-waste-contaminated aquifer waters. Microb Ecol, 44, 95-106.

Bongoua-Devisme, A.J. et al., 2013. Microbial Communities Involved in Fe Reduction and Mobility During Soil Organic Matter (SOM) Mineralization in Two Contrasted Paddy Soils. Geomicrobiology Journal, 30, 347-361.

Canfield, D.E., Glazer, A.N., Falkowski, P.G., 2010. The evolution and future of Earth's nitrogen cycle. Science, 330, 192-196.

Clement, J.C., Shrestha, J., Ehrenfeld, J.G., Jaffe, P.R., 2005. Ammonium oxidation coupled to dissimilatory reduction of iron under anaerobic conditions in wetland soils. Soil Biology & Biochemistry, 37, 2323-2328.

Dalsgaard, T., Canfield, D.E., Petersen, J., Thamdrup, B., Acuña-González, J., 2003. N2 production by the anammox reaction in the anoxic water column of Golfo Dulce, Costa Rica. Nature, 422, 606-608.

Ding, B., Li, Z., Qin, Y., 2017. Nitrogen loss from anaerobic ammonium oxidation coupled to Iron(III) reduction in a riparian zone. Environmental Pollution, 231, 379-386.

Ding, L.J., An, X.L., Li, S., Zhang, G.L., Zhu, Y.G., 2014. Nitrogen Loss through Anaerobic Ammonium Oxidation Coupled to Iron Reduction from Paddy Soils in a Chronosequence. Environmental Science & Technology, 48, 10641-10647.

Guan, Q., 2022. Vertical distribution characteristics and source tracing of organic carbon in sediment of the Yellow River wetland, Sanmenxia, China. Limnologica, 93, 125960.

Guan, Q.S. et al., 2018. Nitrogen loss through anaerobic ammonium oxidation coupled with iron reduction in a mangrove wetland. European Journal of Soil Science, 69, 732-741.

Huang, S., Jaffé, P., Senko, J.M., 2018. Isolation and characterization of an ammonium-oxidizing iron reducer: Acidimicrobiaceae sp. A6. Plos One, 13, 1-12.

Huang, S., Jaffé, P.R., 2015. Characterization of incubation experiments and development of an enrichment culture capable of ammonium oxidation under iron-reducing conditions. Biogeosciences, 12, 769-779.

Jensen, M.M., Kuypers, M.M.M., Lavik, G., Thamdrup, B., 2008. Rates and regulation of anaerobic ammonium oxidation and denitrification in the Black Sea. Limnology and Oceanography, 53, 23-36.

Li, X.F. et al., 2015. Evidence of Nitrogen Loss from Anaerobic Ammonium Oxidation Coupled with Ferric Iron Reduction in an Intertidal Wetland. Environmental Science & Technology, 49, 11560-11568.

Lovley, D.R., Phillips, E.J.P., 1987. Rapid Assay for Microbially Reducible Ferric Iron in Aquatic Sediments. Applied and Environmental Microbiology, 53, 1536-1540.

Melton, E.D., Stief, P., Behrens, S., Kappler, A., Schmidt, C., 2014. High spatial resolution of distribution and interconnections between Fe- and N-redox processes in profundal lake sediments. Environ Microbiol, 16, 3287-303.

https://doi.org/10.5194/egusphere-2022-1209
Preprint. Discussion started: 12 January 2023

Peng, Q.-a. et al., 2016. The diversity of iron reducing bacteria communities in subtropical paddy soils of China. Applied Soil Ecology, 101, 20-27.

Sawayama, S., 2006. Possibility of anoxic ferric ammonium oxidation. Journal of Bioscience and Bioengineering, 101, 70-72.

Shu, D., He, Y., Yue, H., Wang, Q., 2016. Metagenomic and quantitative insights into microbial communities and functional genes of nitrogen and iron cycling in twelve wastewater treatment systems. Chemical Engineering Journal, 290, 21-30.

Somenahally, A.C., Hollister, E.B., Yan, W., Gentry, T.J., Loeppert, R.H., 2011. Water management impacts on arsenic speciation and iron-reducing bacteria in contrasting rice-rhizosphere compartments. Environ Sci Technol, 45, 8328-35.

Thamdrup, B., Dalsgaard, T., 2002. Production of N2 through Anaerobic Ammonium Oxidation Coupled to Nitrate Reduction in Marine Sediments. Applied and Environmental Microbiology, 68, 1312-1318.

Wang, L., Li, T., 2011. Anaerobic ammonium oxidation in constructed wetlands with bio-contact oxidation as pretreatment. Ecological Engineering, 37, 1225-1230.

Weber, K.A., Achenbach, L.A., Coates, J.D., 2006. Microorganisms pumping iron: anaerobic microbial iron oxidation and reduction. Nature Reviews Microbiology, 4, 752-764.

Yang, W.H., Weber, K.A., Silver, W.L., 2012. Nitrogen loss from soil through anaerobic ammonium oxidation coupled to iron reduction. Nature Geoscience, 5, 538-541.

Zhou, G.W. et al., 2016. Electron Shuttles Enhance Anaerobic Ammonium Oxidation Coupled to Iron(III) Reduction. Environmental Science & Technology, 50, 9298-9307.

Appendix I Denitrification and Annamox Rate

For the anammox and denitrification incubations, 100 μL of $Na^{15}NO_3$ (98% ^{15}N, Sigma–Aldrich, St. Louis, MO, USA) were taken extracted and transferred into a vial using a micro-sampling needle. The final $^{15}NO_3^-$ concentration was 100 μmol L^{-1}, and the amount of ^{15}N in the mud was ignored. The culture time was set to 0 h, 8 h, 16 h, 24 h, 48 h, and 72 h. After each time point, the microorganism reaction was terminated by injecting 200 μL of saturated HgCl into the vial. The $^{29}N_2$ and $^{30}N_2$ in the headspace were measured using a GasBench II−Delta V Advantage isotope ratio mass spectrometer (Thermo Fisher, Bremen, Germany). This method was also used to measure the denitrification and anammox rates. The details of these procedures have been reported in previous studies (Thamdrup and Dalsgaard, 2002) Guan, 2019).

The results are shown in Fig. A1, A2, and A3.

https://doi.org/10.5194/egusphere-2022-1209
Preprint. Discussion started: 12 January 2023

The main nitrogen loss in the YJW site was due to denitrification. Anammox was not detected in the YJW site. The maximum denitrification of 1.09 mg N kg^{-1} d^{-1} occurred in the 5–10cm sample. The main nitrogen loss mechanism in the TEH site was anammox. Denitrification was not detected. The maximum anammox of 0.14 mg N kg^{-1} d^{-1} occurred in the 0–5cm sample. The 5–10 cm YJW and 10–13 cm YJW samples had higher denitrification rates than the other layers.

Appendix II The nitrogen-metabolism gene abundance heatmap in the metagenomic group

Nitrogen fixing: nitrogenase; gene: nifH

Nitrification: ammonia monooxygen; gene: amoA

Hydroxylamine oxidoreductase; gene: hao

Nitrite oxidoreductase; gene: nxrA

Denitrification reductase; gene: narG

Nitrite reductase; genes: nirS and nirK

Nitric oxide reductase; gene: norB

Nitrous oxide reductase; gene: nosZ

Anammox: N_2H_4 synthase; gene: hzsA; N_2H_4 oxidoreductase hzo

Nitrogen assimilation reduction: nitrate assimilation reductase; genes: nasA and narB

Nitrite assimilation reductase; genes: nirA and nirB

Nitrogen dissimilatory reduction (DNRA): nitrate dissimilatory reductase; gene: napA

Nitrite dissimilary reductase; gene: nrfA

Ammonation: urease; gene: ureC

https://doi.org/10.5194/egusphere-2022-1209
Preprint. Discussion started: 12 January 2023

https://doi.org/10.5194/egusphere-2022-1209
Preprint. Discussion started: 12 January 2023

411

Table 1: Characteristics of water*

Site	Temperature	Conductivity (μS cm^{-1})	pH	Eh (mV)	DO	NO_3^--N (mg L^{-1})	NO_2^--N (mg L^{-1})	NH_4^+-N (mg L^{-1})	TP (mg L^{-1})	TFe (mg L^{-1})	Fe(II) (mg L^{-1})	Fe(III) (mg L^{-1})	SS (g L^{-1})
YJW	30.60±0.81a	907±41a	8.59±0.03a	216±13a	6.94±0.32a	1.58±0.03a	0.13±0.34a	0.04±0.00a	0.07±0.00a	0.08±0.01a	0.04±0.01a	0.04±0.00a	0.28±0.01a
TEH	32.90±1.13a	885±28a	8.29±0.03a	164±5b	6.38±0.21a	1.55±0.03a	0.02±0.00b	0.05±0.01a	0.06±0.00a	0.05±0.00b	0.04±0.00a	0.01±0.00b	2.04±0.01b

*n=3, the same letter indicates no significant difference at $p<0.05$.

412

413

https://doi.org/10.5194/egusphere-2022-1209
Preprint. Discussion started: 12 January 2023

414

Table 2: Chemical characteristics of sediments*

Site	Depth (cm)	pH	TOC (%)	TN (%)	NO_3^--N (mg kg^{-1})	NO_2^--N (mg kg^{-1})	NH_4^+-N (mg kg^{-1})	TFe (mg kg^{-1})	Fe(II) (mg kg^{-1})	Fe(III) (mg kg^{-1})	Moisture content (%)
YJW	0–5	8.97	0.22	0.06	1.39±0.22d	0.031±0.008c	14.36±0.67a	64±14b	4±0.8d	60±14b	21.02
	5–10	8.73	0.27	0.05	0.93±0.01e	0.040±0.000b	16.47±0.77a	108±2a	30±3.0b	78±21a	23.60
	10–13	8.83	0.28	0.05	1.33±0.27d	0.046±0.000b	14.28±1.02a	110±0a	66±6.6a	44±6.6c	24.04
	13–18	9.00	0.03	0.02	0.92±0.05e	0.030±0.004c	3.62±0.18d	13±0c	6±0.2c	7±0.56d	5.69
TEH	0–5	8.80	0.38	0.06	7.51±0.97a	0.370±0.010a	6.27±0.36b	5±0.5d	4±0.6d	1±0.54f	3.44
	5–10	8.86	0.48	0.08	3.23±0.12c	0.037±0.001c	4.33±0.53c	6.4±2.4d	4.4±0.7d	2±1.70e	10.10
	10–20	8.84	0.41	0.07	0.60±0.00f	0.041±0.000b	5.39±0.54b	0.28±0.08f	0.17±0.03e	0.11±0.09g	13.04
	20–30	8.75	0.26	0.03	4.27±0.11b	0.040±0.001b	5.51±0.72b	1.17±0.3e	0.22±0.16e	0.95±0.50f	12.66

*n=3, the same letter indicates no significant difference at $p<0.05$.

415

416

https://doi.org/10.5194/egusphere-2022-1209
Preprint. Discussion started: 12 January 2023

417

Table 3: Possible processes of $^{29}N_2$ and $^{30}N_2$ generation from $^{15}NH_4^+$ under anaerobic conditions

Product	Nitrogen substrate 1	Nitrogen substrate 2	Process
$^{30}N_2$	Added $^{15}NH_4^+$	Added $^{15}NH_4^+$	Feammox to N_2
	Added $^{15}NH_4^+$	Feammox-generated $^{15}NO_2^-$ and $^{15}NO_3^-$	Anammox
	Feammox-generated $^{15}NO_2^-$ and $^{15}NO_3^-$	Feammox−generated $^{15}NO_2^-$ and $^{15}NO_3^-$	Denitrification
$^{29}N_2$	Added $^{15}NH_4^+$	Background $^{14}NH_4^+$	Feammox to N_2
	Added $^{15}NH_4^+$	Feammox-generated $^{14}NO_2^-$ and $^{14}NO_3^-$	Anammox
	Feammox-generated $^{15}NO_2^-$ and $^{15}NO_3^-$	Background $^{14}NH_4^+$	Anammox
	Feammox-generated $^{15}NO_2^-$ and $^{15}NO_3^-$	Feammox-generated $^{14}NO_2^-$ and $^{14}NO_3^-$	Denitrification

418

419

https://doi.org/10.5194/egusphere-2022-1209
Preprint. Discussion started: 12 January 2023

420

Table 4: The rates of Feammox and ecosystem nitrogen loss in different types of soils

Types	Feammox rates (mg N kg^{-1} d^{-1})	Nitrogen loss through Feammox (t N km^{-2} a^{-1})	Reference
Yellow River wetland	0.02–0.13	1.1–7.1 (0–10 cm)	This study
Tropical forest soils	0.32	0.1–0.4 (0–10 cm)	(Yang et al., 2012)
Paddy soils	0.17–0.59	0.78–6.1 (0–10 cm)	(Ding et al., 2014)
Yangtze Estuary	0.24–0.36	11.5–18 (0–5 cm)	(Li et al., 2015)
Riparian zone	0.32–0.37	2.4–4.4 (0–10 cm)	(Ding et al., 2017)
Mangrove	0.38–0.48	6.26 (0–5 cm)	(Guan et al., 2018)

421

422

https://doi.org/10.5194/egusphere-2022-1209
Preprint. Discussion started: 12 January 2023

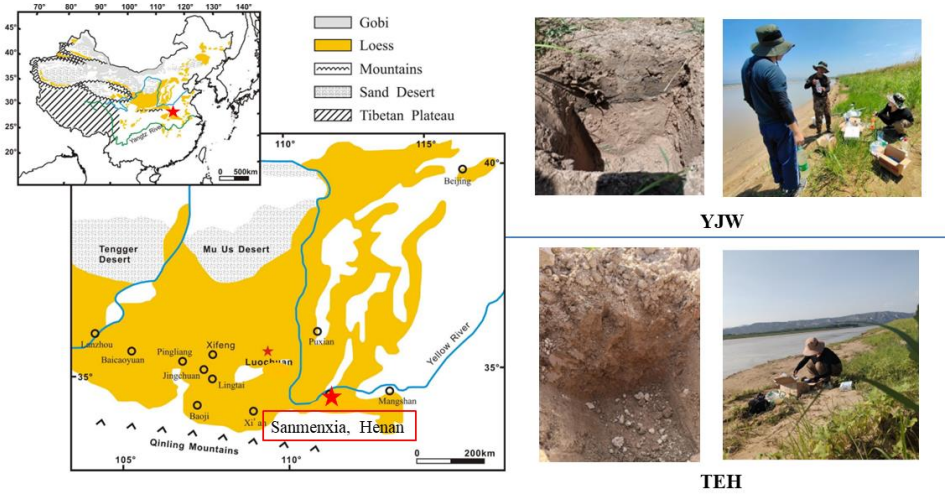

423

424 Figure 1

425

https://doi.org/10.5194/egusphere-2022-1209
Preprint. Discussion started: 12 January 2023

426

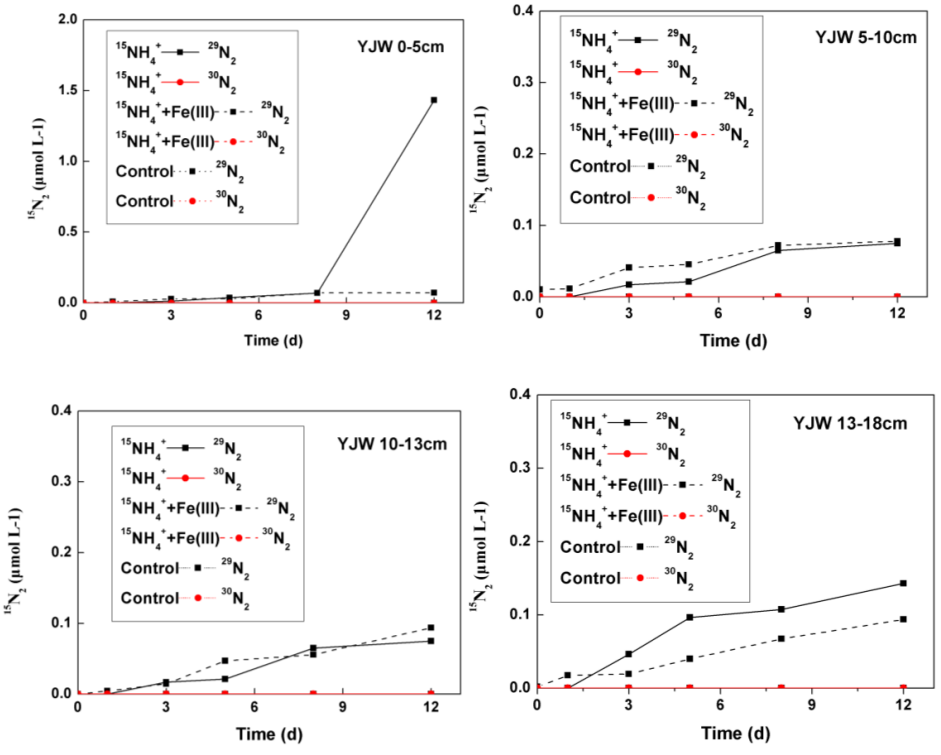

427

428

429 Figure 2

430

https://doi.org/10.5194/egusphere-2022-1209
Preprint. Discussion started: 12 January 2023

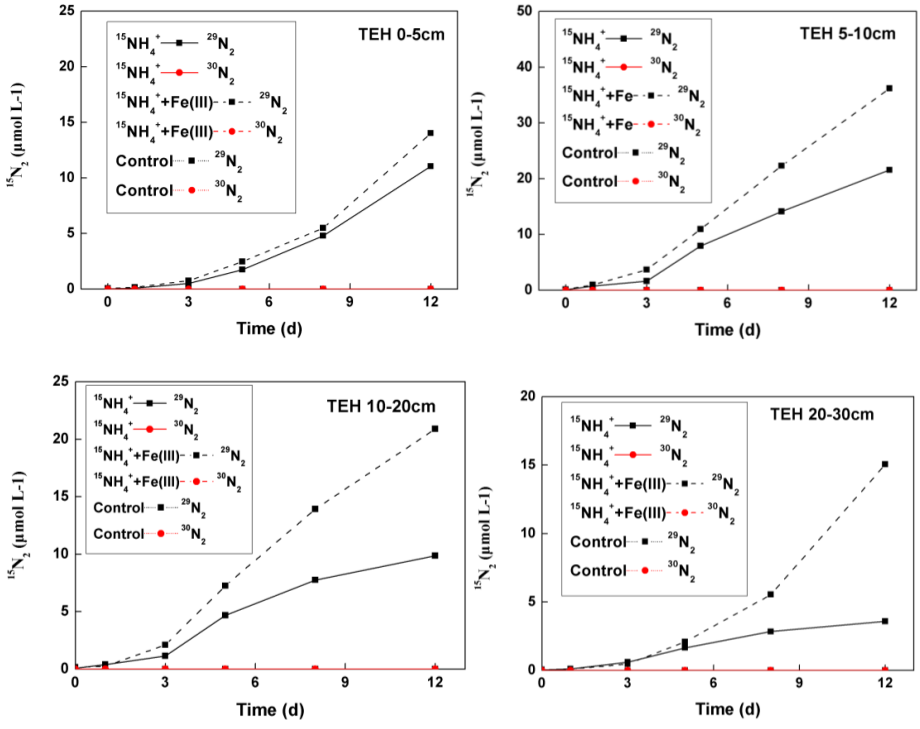

Figure 3

https://doi.org/10.5194/egusphere-2022-1209
Preprint. Discussion started: 12 January 2023

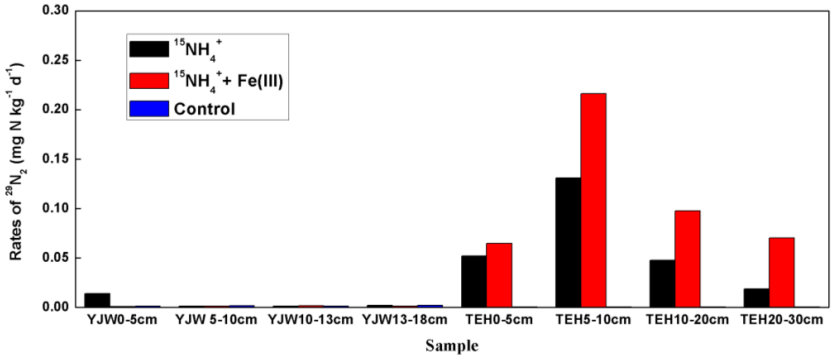

435

436 Figure 4

437

https://doi.org/10.5194/egusphere-2022-1209
Preprint. Discussion started: 12 January 2023

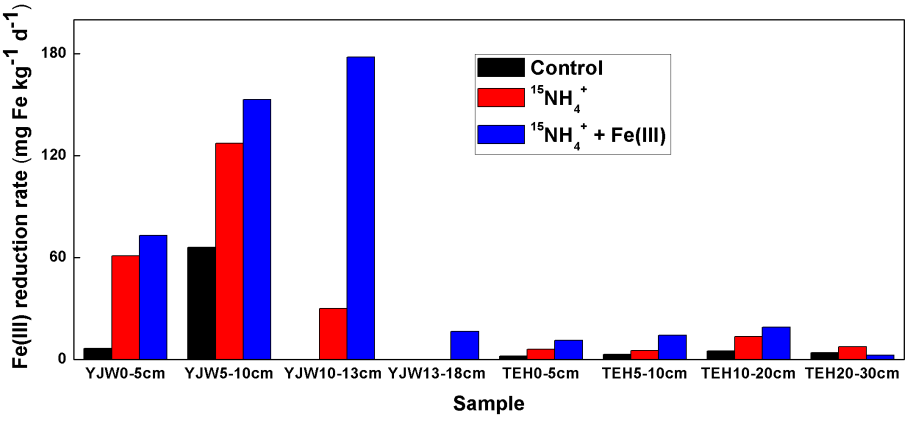

438

439 Figure 5

440

https://doi.org/10.5194/egusphere-2022-1209
Preprint. Discussion started: 12 January 2023

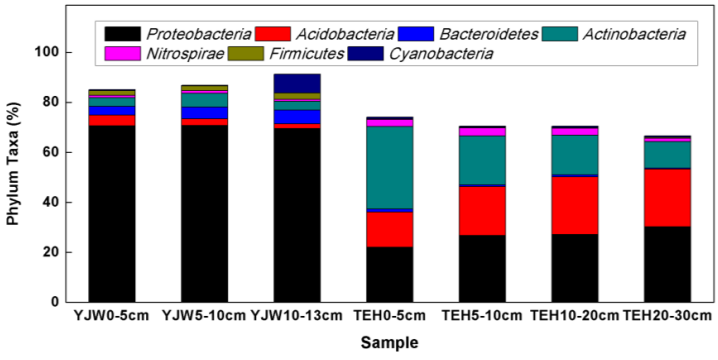

441

442 Figure 6

443

https://doi.org/10.5194/egusphere-2022-1209
Preprint. Discussion started: 12 January 2023

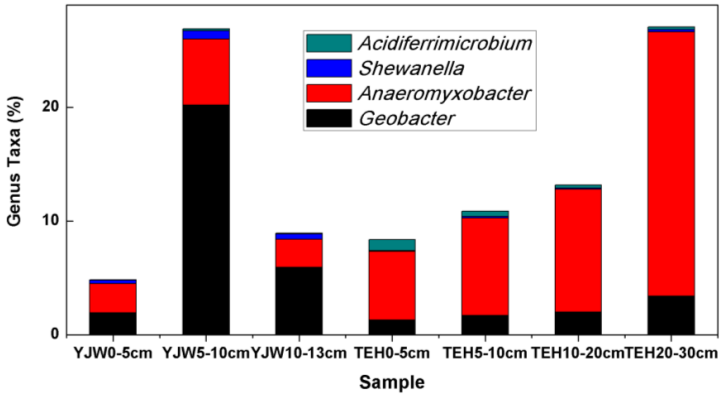

444

445 Figure 7

446

https://doi.org/10.5194/egusphere-2022-1209
Preprint. Discussion started: 12 January 2023

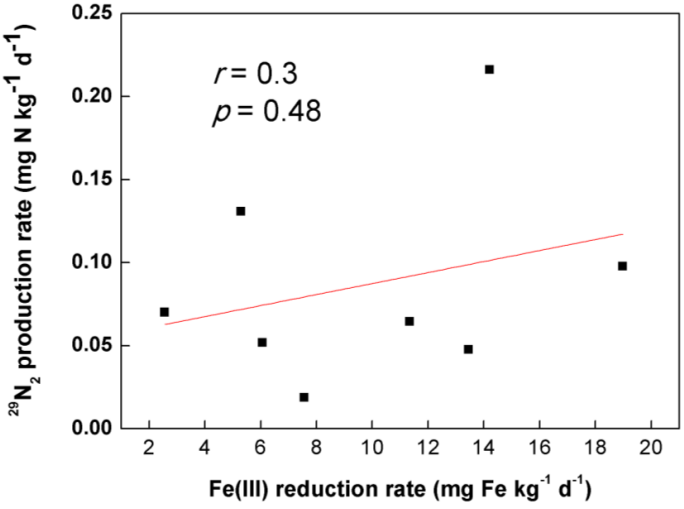

447

448 Figure 8

449

https://doi.org/10.5194/egusphere-2022-1209
Preprint. Discussion started: 12 January 2023

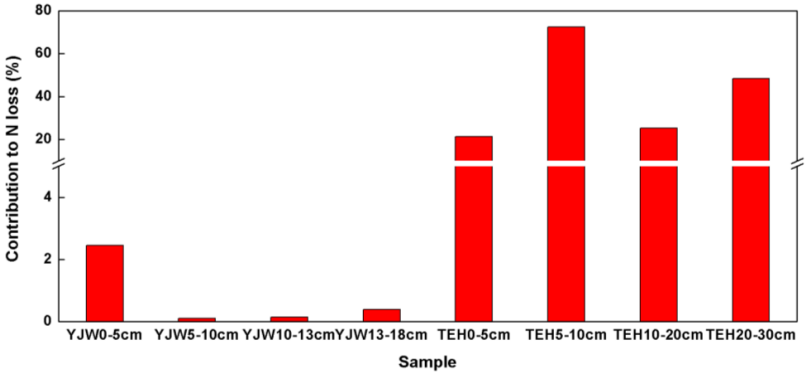

Figure 9

https://doi.org/10.5194/egusphere-2022-1209
Preprint. Discussion started: 12 January 2023

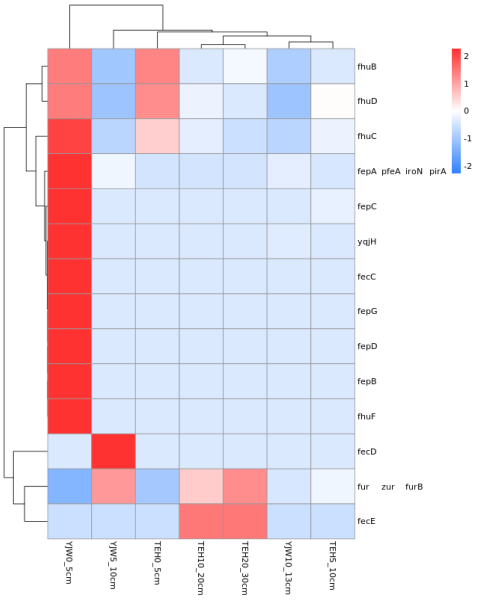

453

454 Figure 10

455

https://doi.org/10.5194/egusphere-2022-1209
Preprint. Discussion started: 12 January 2023

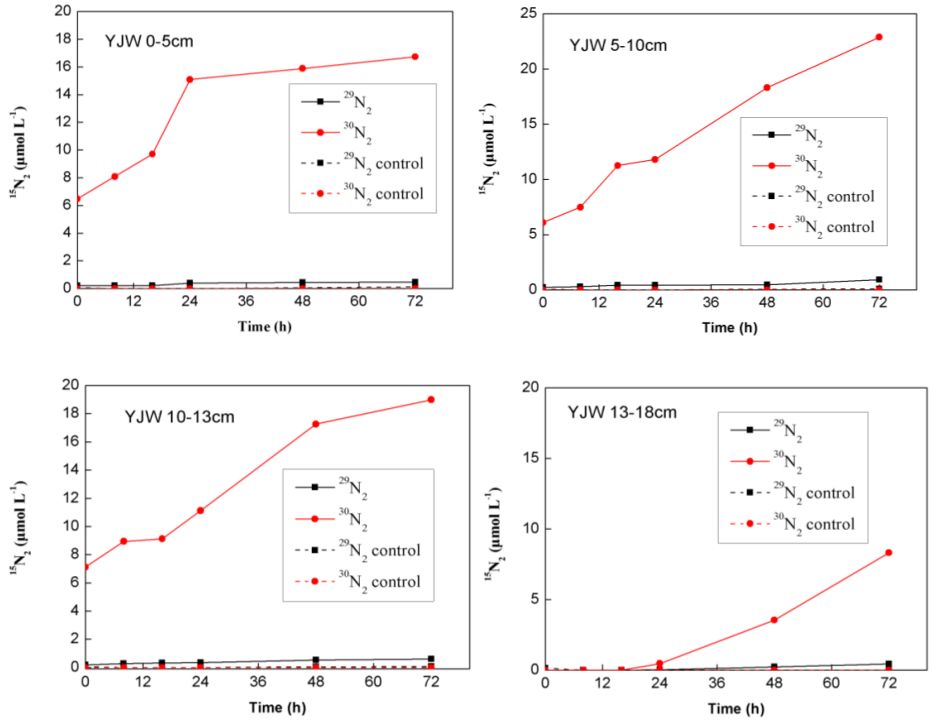

Figure A1

https://doi.org/10.5194/egusphere-2022-1209
Preprint. Discussion started: 12 January 2023

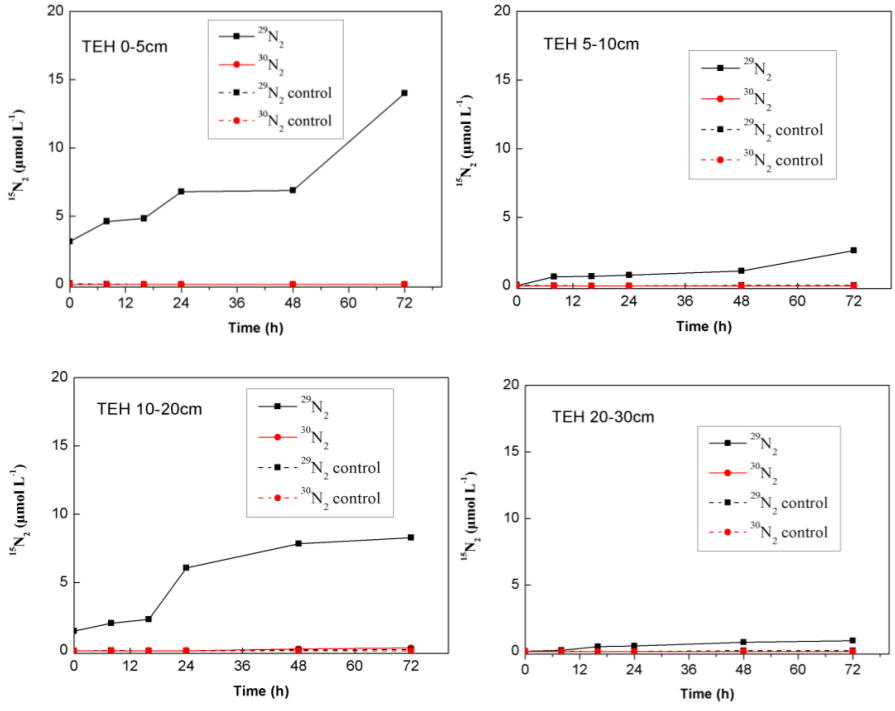

Figure A2

https://doi.org/10.5194/egusphere-2022-1209
Preprint. Discussion started: 12 January 2023

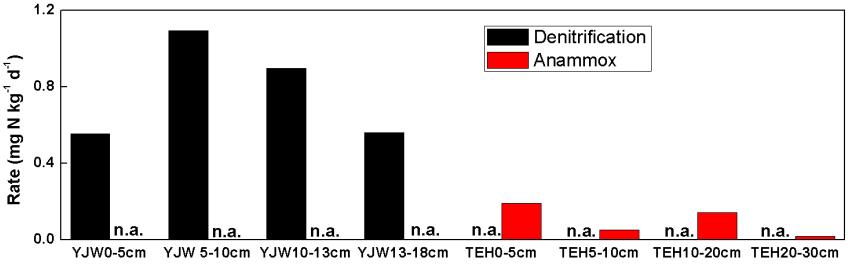

Figure A3

https://doi.org/10.5194/egusphere-2022-1209
Preprint. Discussion started: 12 January 2023

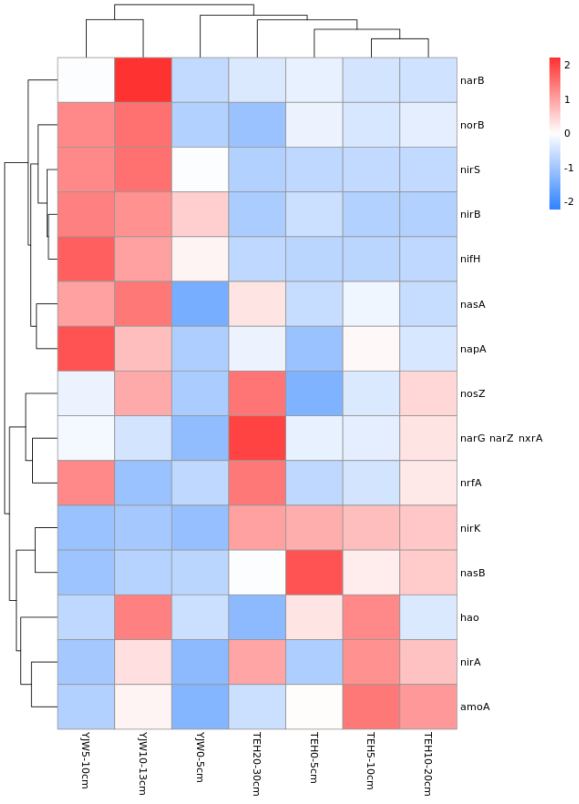

Figure A4